Fundamental study of shock/shock interference in low density flow : flowfield measurements by DLCARS.

T. Pot, B. Chanetz, M. Lefebvre and P. Bouchardy
ONERA, Chatillon, France

1 Introduction

This study of shock/shock interference has been undertaken in the framework of the Program of Research For Advanced Hypersonic Propulsion decided by the French Ministry of Defence. The aim of this program is to conceive a scramjet for hypersonic applications. For this project -as far as external aerodynamics is concerned- one of the most challenging problem is the definition of air intakes. Indeed the shocks produced by the compression ramps intersect the shock forming ahead of the cowl, whose profile is blunt so as to limit the heat flux. The shock/shock interferences thus can produce locally spectacular heat flux and pressure increases. Therefore it is important to know the phenomena involved in these shock/shock interferences. Edney [1] by analysing carefully his own experiments has defined six types of basic interference. The terminology he then introduced in order to classify them has been adopted universally. To introduce the different interferences, we shall consider an oblique shock C_1 meeting the detached shock C_2, which forms ahead of a blunt obstacle.
When the oblique shock crosses the bow shock in the area where it is a strong shock, the two shocks have very different intensities, and a slip line results from this interference, separating a region above this line where the flow is subsonic, with low velocity, from a region underneath with supersonic flow and high velocity. When the reattachment of the slip line is possible on the obstacle, the situation is called type III interference. When it is impossible, the slip line is followed by a supersonic jet surrounded by a subsonic flow. When the supersonic jet impacts the cylinder, the situation corresponds to type IV interference.
The air intake situation is simulated very schematically by a shock generator which produces a weak oblique shock and a cylinder located perpendicularly to the free stream flowfield direction. The aim of this experiment being the furniture of a test-case for numerical applications, the choice has been done to perform experiments at low Reynolds number to avoid to take into account a turbulence modelisation.
Three configurations have been tested : the reference case with a cylinder alone in

the flow producing a bow shock, type III and type IV interference cases obtained by adding a shock generator in front of the cylinder to obtain an impinging shock meeting the bow shock.
This paper is divided in two parts :

- The first part is devoted to the presentation of the experimental set-up, the facility used and the description of the measurement techniques employed.
- The second part is relative to the three configurations analysed.

2 Experimental arrangement, visualizations and measurement techniques

2.1 The R5Ch facility

The experimental study has been carried out in the R5Ch blow-down wind tunnel located in the ONERA Chalais-Meudon research center near Paris. The facility, where stagnation temperature and pressure are 1070 K and 2.5×10^5 Pa respectively, produces a uniform flow at Mach number 10. The free stream static conditions are $p_0 = 6.3$ Pa ; $T_0 = 52$ K and $\rho_0 = 4.3$ kg.m^{-3}. Because of the low stagnation pressure, the unit Reynolds number is $Re_u = 167,000/\text{m}$.
Thanks to the diffuser efficiency and to the large capacity of the vaccuum sphere - the volume of which being equal to 500 m^3 -the run duration is comprised between 60 and 90 seconds depending of the model placed in the test-section.

2.2 Models and equipment

The shock generator is an isosceles triangle, the base of which being equal to 100×10^{-3}m. The leading edge angle is $10°$. The rotation possibility of the generator (see Fig. 1) allows a variation of the shock intensity. The cylinder located downstream of the shock generator has a diameter $\phi = 16 \times 10^{-3}$m. It is positioned perpendicular to the free stream flow. Its spanwise length is $L = 100 \times 10^{-3}$m like the generator's span. The ratio of the spanwise length to the diameter is higher than 6, which is sufficient to insure a two dimensional flow in the middle of the cylinder in the domain where the thermocouple and pressure taps are located.

Two models have been built. The first with two pressure taps lines located in the middle of the cylinder and separated by 18 mm. Because of the low static pressure of the free flow ($p_0 = 5.9$ Pa), particular care was taken in measuring the surface pressures. The method used consisted of employing differential sensors with inductance variation, type Validyne DP45. Two membrane types were used : type 6-20 for a pressure range between 0 and 860 Pa and type 6-30 for a pressure range between 0 and 8600 Pa in the region of interaction. For the measurement,

a zero pressure reference -obtained by a turbo molecular pump- is applied to one side of the transducer.
The second model is equipped with thermocouples on two lines as for pressure model. Heat flux have been measured by the "thick skin method" [2]. It consists in the measurement of model surface temperature increase. The thermometric element is composed of a 0.15 mm Chromel wire inserted in a steel ISOTAN plot. The plot is included in the model, itself realized in ISOTAN.
The thermocouple obtained (type E) has a mean sensitivity equal to 60μV/K. The temperature is recorded at a 100 Hz frequency during the first five seconds of the run. From the parabolic evolution of temperature with respect to the time, the heat-flux is deduced. In fact the determination of the heat-flux is performed during the first half second of the run, so that any lateral conduction could be neglected.

2.3 CARS techniques

Dual-line Coherent Anti Stokes Scattering (DL-CARS) is a technique which has been proposed and previously tested to perform instantaneous measurements of temperature and density in low-pressure supersonic flows [3],[4].
Figure 2 shows the frequency diagram involved in DL-CARS. Three laser beams of frequency $\omega_1, \omega_2, \omega'_3$ are required. These frequencies are adjusted so that $(\omega_1 - \omega_2)$ and $(\omega_1 - \omega'_2)$ are resonant with two different Q Raman lines with frequencies ω_J and ω'_J. Thus, two CARS signals are simultaneously produced at frequencies $\omega_3 = \omega_1 + \omega_J$ and $\omega'_3 = \omega_1 + \omega'_J$. On the hand, the rotationnal temperature is deduced from the ratio of the intensities of the two Raman lines, assuming a Boltzman equilibrium between the rotational level manifold. On the other hand, the gas density is got from the absolute intensity of one Raman line or both, after calibrating the optical response at the spectral position of each Raman line. The laser beams are delivered from one optical bench equipped with a seeded Nd YAG laser and a dye chain producing 12 ns long pulse duration at a repetition rate of 12.5 Hz. At the output, the avaible energies are 40 mJ at the frequency ω_1, i.e λ_1 = 532 nm and 0.7 mJ at frequencies ω_2 and ω'_2, around 607 nm. The beams are developped successively in the test chamber of the R5Ch wind tunnel and in a reference cell, using the folded boxcar configuration [5]. In the test chamber, the CARS signals are generated from the probe volume which is 40 mm long and 0.2 mm in diameter; the axis of the probe volume is perpendicular to the direction of the Mach 10 flow. So the spatial resolution is 0.2 mm in the direction of the strongest gradient.
During a run, six positions separated of 0.5 mm from each others are probed. For each position, 120 laser shots are averaged to increase the number of collected photelectrons, limiting so the shot noise influence. In such conditions, the relative precision on temperature and density is better than 7% and 10% respectively.

3 Presentation of the results

3.1 Reference case : cylinder alone in the flow

This case has been carefully characterized by measuring pressure and heat-flux at the wall. The detached shock region in front of the cylinder has been probed by DLCARS. Figure 3 shows the evolution of rotation temperature along the stagnation line. Since in the R5Ch conditions, rotation equilibrium is recovered after a few collision between molecules, the rotation temperature is equal here to the static temperature. The temperature jump due to the shock, particularly intense at large Mach number, is in good agreement with the numerical results obtained with ONERA-Homard2 solver [4].
Density, deduced from the CARS probing along the stagnation line, is presented in figure 4. The good agreement between calculation and experiment leads to two conclusions :

- the validity of the measurement technique
- the accuracy of the continuum approach used to solve the conservation equation for mass momentum and energy (Navier-Stokes equations).

3.2 Type III interference

Figure 5 shows a visualization of the flow obtained thanks to Electron Beam Fluorescence (EBF). The incident shock wave meets the detached shock wave by modifying deeply its structure, since in the upper part the shock detachment distance increases and reaches twice the reference case value ($\Delta/R = 0,72$ in type III pattern instead of $\Delta/R = 0,37$ in the reference case).
As far as shock/shock interferences are concerned, the most spectacular effect is the existence of pressure and heat-flux peaks at the wall due to the impact of shear layer (type III) or supersonic jet (type IV). Therefore, Edney titled in 1968 his report [1] : "*Anomalous* heat transfer and pressure distributions on blunt bodies at hypersonic speeds in the presence of an impinging shock". Figure 6 presents the evolution of pressure around the cylinder in the reference case and in the two studied interference types. The pressures are divided by the pressure at the cylinder stagnation point (p_{ref}) in the reference case. The curve relative to type III interference exhibits a pressure peak at $\theta = -45°$ $p_{pk}/p_{ref} = 2.6$.
Figure 7 shows the heat flux distribution along the cylinder. The results are divided by Φ_{ref} = 65000 W/m^2, which is the experimental value obtained at the stagnation point on the cylinder in the reference case without impinging shock. The heat flux peak observed in this figure is three times higher than the heat flux measured at the stagnation point in the reference case.

3.3 Type IV interference

Figure 8 shows the type IV pattern obtained by Electron Bean Fluorescency (EBF). The cylinder is located more downstream of the shock generator than in the former case (type III). Thus the impinging shock meets the bow shock in the aera where it is nearly normal as it is represented in figure 9. The two shocks thus have very different intensities and the slip line resulting from the interference cannot reattach and a supersonic jet impacts the wall. The consequence of the impact is important in term of pressure and heat-flux as it is pointed out by figures 6 and 7. The pressure peak reaches 7.6 at $\theta = -25°$. The Mach number downstream of incident shock ($C1$) is $M_1 = 4.22$. Behind the shock ($C3$), the Mach number is only $M_3 = 2.73$. The image of the triple point I_1, intersection of the three shocks is represented in figure 10 at the intersection of the three polars M_0, M_1 and M_3. At the impact point R between shear layer (Σ_1) and the cylinder, the flow comprised between (Σ_1) and the shock ($C3$) undergoes a deviation Σ_3 associated to a shock wave ($C4$) which intersects ($C3$) in a second triple point I_2. The shock (C_5) is more intense so that the flow behing it is subsonic. But downstream the shock (C_4) the flow is supersonic so that a supersonic jet is limited by two boundaries (f_1) on the side *(5)* and (f_2) on the side *(2)*. Thus the supersonic jet is a succession of compression and expansion waves represented in the shock polar plane by portions of isentropic polars (Fig. 10).
In addition wall measurements, DLCARS technique has been used to qualify the flow. Rotation temperatue and nitrogen number density have been measured along 9 lines in front of the cylinder, constituting a total of 125 points.
The line located at Y = 4.5 mm under the stagnation line is presented in figure 11. This line is located under the slip line and the supersonic jet. It crosses the shock wave emanating from the second triple point I_2. Therefore in figure 11, one notes a temperature jump due to the shock at X = 2 mm. A correlative density increase is observed at the same abscissa (Fig. 11). The maximum reaches 9×10^{-3} kg/m^3 which is more than twenty times the value of the density in the upstream flow ($\rho_0 = 0.4 \times 10^{-3}$ kg/m^3). Through a normal shock wave at Mach 10, the specific mass increase is nearly equal to six times the upstream value. Thus the density increase is much more important in shock/shock interference pattern than in a bow shock. For this reason the flow after the shocks is more energetic and induces large heat flux peaks at the wall. The phenomenon has been well quantified thanks to CARS.

4 Conclusion

The work was devoted to an experimental study of shock/shock interference performed in a blow-down wind tunnel. Three configurations were tested : the reference case with a cylinder alone in the flow giving a bow shock, type III and type IV interference cases obtained by adding a shock generator in front of the cylinder to

obtain an impinging shock meeting the bow shock. The experiment constitutes a well documented test-case useful for the validation of Computation Fluid Dynamics (CFD) solvers. It has been selected in the first Eastern-Western High Speed FlowField (HSFF) Data Base Workshop which will be held in Kyoto (Japan) in November 1998.

References

[1] Edney B., *Anomalous heat transfer and pressure distributions on blunt bodies at hypersonic speeds in the presence of an impinging shock.*, Aeronautical research institute of Sweden, report 115, Stockholm (1968). 1, 4

[2] Consigny H., Mentré V. and Bétrémieux A. *Méthode de mesure de flux de convection dans les souffleries R2 et R3 de Chalais-Meudon. Mise en œuvre actuelle et développements envisagés.*, Colloque AAAF, Poitiers, 26-28 octobre 1987. 3

[3] Péalat M., Lefebvre M., *Temperature measurements by single-shot dual-line CARS in a low pressure flow.*, Applied Physics B, 53,23 (1991). 3

[4] Grisch F., Bouchardy P., Péalat M., Chanetz B., Pot T., Coët M.C. *Rotational Temperature and density measurement in a hypersonic flow by dual line CARS.*, Applied Physics, B56, 14 (1993). 3, 4

[5] Prior Y., *Three dimensionnal phase matching in four wave-mixing*, Applied Optics, 19, 1741 (1980). 3

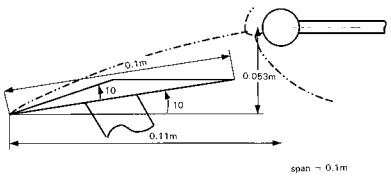

Figure 1: Experimental set up

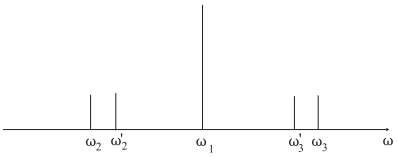

Figure 2: Frequency diagram involved in DL-CARS

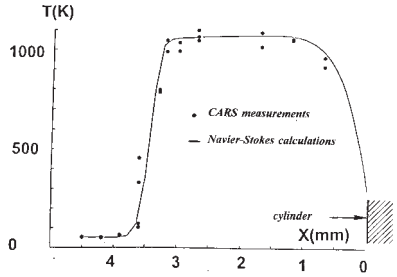

Figure 3: Evolution of the temperature on the stagnation line

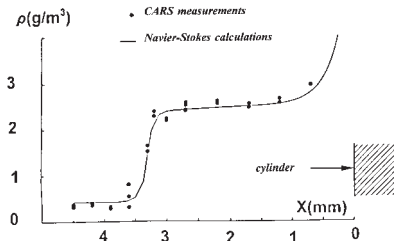

Figure 4: Evolution of the density on the stagnation line without interaction

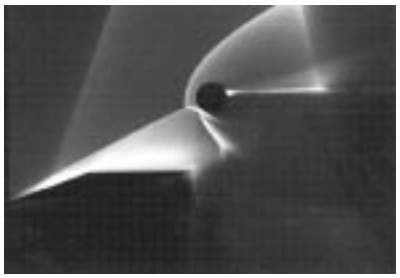

Figure 5: Visualization of the type III interaction by EBF

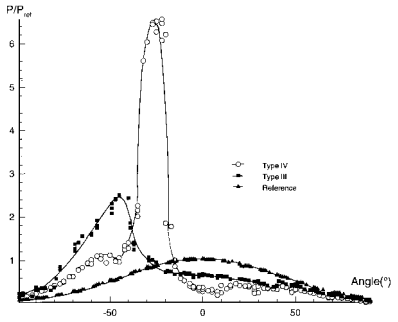

Figure 6: Pressure distribution around the cylinder

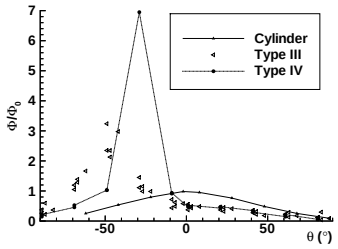

Figure 7: Flux distribution around the cylinder

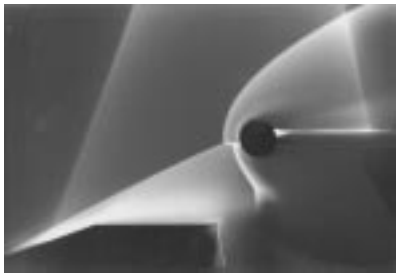

Figure 8: Visualization of the type IV interaction by EBF

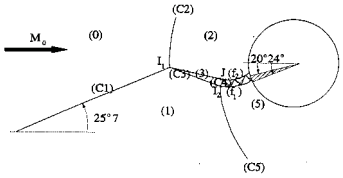

Figure 9: Scheme of the Type IV interaction

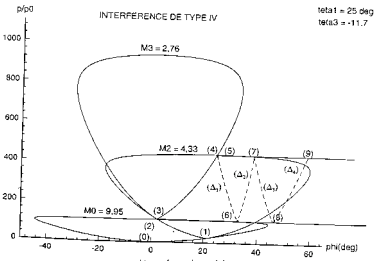

Figure 10: Polar shock of the type IV interaction

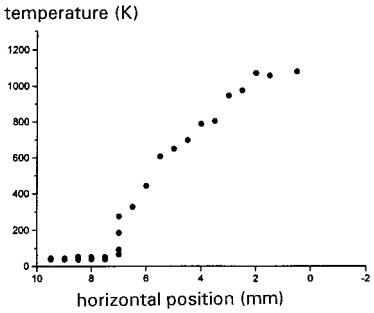

Figure 11: Temperature on the line 4.5 mm under the stagnation line in the case of a Type IV interaction

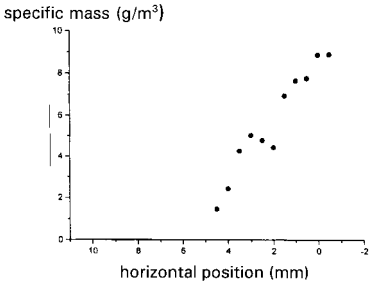

Figure 12: Density on the line 4.5 mm under the stagnation line in the case of a Type IV interaction